Sensors and Actuators B 249 (2017) 321–330

Contents lists available at ScienceDirect

Sensors and Actuators B: Chemical

journal homepage: www.elsevier.com/locate/snb

Amperometric glucose biosensor based on immobilization of glucose oxidase on a magnetic glassy carbon electrode modified with a novel magnetic nanocomposite

Mehdi Baghayeri [a,*], Hojat Veisi [b], Masoud Ghanei-Motlagh [c]

[a] Department of Chemistry, Faculty of Science, Hakim Sabzevari University, P.O. Box 397, Sabzevar, Iran
[b] Department of Chemistry, Payame Noor University, Tehran, Iran
[c] Department of Chemistry, Faculty of Sciences, Shahid Bahonar University of Kerman, Kerman, Iran

ARTICLE INFO

Article history:
Received 27 December 2016
Received in revised form 23 March 2017
Accepted 16 April 2017
Available online 19 April 2017

Keywords:
Diabetes
Direct electron transfer
Silver nanoparticles
Glucose oxidase
Nanocomposite

ABSTRACT

We present a method to produce a magnetic glassy carbon electrode (MGCE) modified with multilayer nanocomposite (Ag@MWCNT-IL-Fe_3O_4) as an immobilization support to promote electron transfer reactions of glucose oxidase (GOx). The nanocomposite verified by transmission electron microscopy (TEM), Fourier transform infrared spectroscopy (FTIR), scanning electron microscopy (SEM), X-ray diffraction (XRD) and a vibrating sample magnetometer (VSM). The direct electron transfer (DET) between GOx and Ag@MWCNT-IL-Fe_3O_4 nanocomposite was investigated using cyclic voltammetry which showed a pair of well-defined redox peaks corresponding to redox active center of GOx. Utilization of constructed electrode for detection of glucose was studied in N_2 and air saturated solutions (pH 7.0). The GOx/Ag@MWCNT-IL-Fe_3O_4/MGCE showed excellent stability, a detection limit of 2.12 μM, a linear range between 6 μM and 2 mM, and a dynamic range up to 2.7 mM at the air saturated solutions. Also, in N_2 saturated solutions (pH 7.0), determination of glucose was carried out by amperometry, and the proposed biosensor showed good reproducibility and stability with a detection limit of 3.8 μM and a linear range between 10 μM and 1 mM. Such analytical performances confirm that the fabricated biosensor used in this work has potential to be applied for development of redox enzyme based biosensors.

1. Introduction

Diabetes mellitus has attracted high attention as public health problem at the worldwide. According to the reports of International Diabetes Federation (IDF) Diabetes Atlas, 342000 people in the Middle East and North Africa Region aged 20–79 died from diabetes and 5.0 million deaths worldwide occurred due to diabetes in 2015, equivalent to one death every six seconds [1]. The primary emphasis of the diagnosis and management of diabetes focuses on trying to test blood glucose levels one to several times in a day. Consequently, it is necessary to develop the glucose sensors and biosensors for the exact detection of glucose levels at biological samples. In common conventional glucose sensors, enzymatic reactions, mainly based on glucose oxidase (GOx), often play the main role. In actual, GOx acts as an "ideal" enzyme at glucose biosensors because of its low cost, high specific activity and reliability [2]. Nevertheless, GOx has some drawbacks. GOx belongs to the class of intrinsic redox enzymes with the catalytic center buried deeply inside the protein shell [3]. Thus, it is extremely difficult to obtain electron transfer (DET) between enzymes and electrode surfaces, so that promoters and mediators are needed to obtain their electrochemical responses [4,5]. Consideration to DET of immobilized GOx in biosensor structure is one of biggest challenges at development of new glucose biosensors, which facilitates enabling fast and significance diagnosis at the third-generation glucose biosensors [6]. Third-generation glucose biosensors involve "wiring" an enzyme to the electrode by co-immobilizing the enzyme and mediator directly onto the electrode surface or into an adjacent matrix such as a conductive polymer film [7,8]. The immobilized mediators act as non-diffusion redox relay stations, effectively facilitating the transport of electrons from the enzyme active site to the electrode [9]. In recent years, the fast development of nanotechnology offers new possibilities to design and fabricate mediator materials

* Corresponding author.
E-mail addresses: m.baghayeri@hsu.ac.ir, mehdi.baghayeri@yahoo.com (M. Baghayeri).

http://dx.doi.org/10.1016/j.snb.2017.04.100
0925-4005/

with high performance to promote DET [10]. Numerous studies also found that nanomaterials of various shapes, sizes, and compositions could improve the performance of electrochemical biosensors and significantly increase the electrical conductivity [11–13]. With manipulated composition and surface modification, nanomaterials such as, magnetic particles [14,15], metal nanoparticles [16,17] and carbon nanotubes (CNTs) [18,19] can be used in fabrication of novel biosensors. In consequence of developments within nanotechnology, the application of metallic nanoparticles in sensing products is rapidly increasing [20]. Among the metallic nanoparticles, silver nanoparticles (AgNPs) are being used in numerous fields due to their conductive and antimicrobial properties [21,22]. The releases of Ag+ ions from silver rich surfaces produce significant antibacterial and cytotoxic effects in several biological medium. There are over 438 products available on the open market that contain AgNPs [20,23]. In recent years, AgNPs have been widely employed for the improvement of sensing properties in the sensors and biosensors [24], development in the detection of DNA [25] and cancer [26]. In the last two decade, numerous studies have utilized CNTs in bioapplications ranging from the cancer biomarkers [27] to biosensing applications for a host of biomolecules [28] and even for the field of genetics [29]. Literature survey have proved that the combination of CNTs with nanomaterials such as nanoparticles, thus developing CNTs-nanoparticle hybrid nanostructures, presents several extra unique physicochemical properties and utilities that are both highly necessary and noticeably helpful for bio-applications compared with either material alone [30–32]. Furthermore, such matrices can well become incorporated in a clinical and laboratory diagnostic tools because they have some advantages such as high surface area, unique catalyst activities, good stability and excellent electrical conductivity [33]. Fe_3O_4 nanoparticles, also known as biomolecule carriers, are typically magnetic nanoparticles with biosensing applications [31]. Extensive research efforts were recently directed towards the application of Fe_3O_4 nanoparticles as magnetic loaders with the help of external magnetic field. In biosensing platforms, the synergic effect of nanoparticles with other material, which have excellent conductivity and catalytic properties, can provide the necessary conduction pathways for electrons on the electrode surface to increase current signal. Room temperature ionic liquids (ILs) are very good candidate that can be applied in electrochemical biosensors and have presented superior electrochemical performances as a result of their profit, such as good conductivity, wide electrochemical windows, low volatility, appropriate chemical properties and good thermal characteristic [34]. The functionalization of Fe_3O_4 nanoparticles with ILs opens a new way to development of novel and efficient approaches for the combination of the very small building blocks of biosensors into desired structures. To the best of our knowledge, there are few well-defined reports about such structures.

In the present work, we report a novel multilayer nanocomposite Ag@MWCNT-IL-Fe_3O_4 for fabrication of third-generation biosensors. MWCNT-IL-Fe_3O_4 composite has been consisted from MWCNTs orderly assembled on functionalized positions of Fe_3O_4 nanoparticles (Fe_3O_4 NPs) with ILs. The main novelty of our MWCNT-IL-Fe_3O_4 nanocomposite mainly includes the following points: (1) the high magnetic properties of MWCNT-IL-Fe_3O_4 nanocomposites makes it as a good matrix for stable immobilization on magnetic glassy carbon electrode (MGCE) surface, and (2) functional groups on the MWCNT are ideal reaction sites for the electrodeposition of other nanoparticles (here AgNPs) and thus provide an appropriate approach for enzyme immobilization. Herein, the proposed Ag@MWCNT-IL-Fe_3O_4 nanocomposite supplied a unique interfacial microenvironment for GOx, which could accelerate the DET at the electrode surface.

2. Experimental section

2.1. Materials

The chemicals, GOx (Aspergillusniger, EC 1.1.3.4. 150,000 unit/g) and glucose (Sigma, 99%) were obtained from USA and used without additional purification. Ferric chloride hexahydrate ($FeCl_3{\cdot}6H_2O$), ferrous chloride tetrahydrate ($FeCl_2{\cdot}4H_2O$), and all solvents were purchased from Merck (Darmstadt, Germany) and were used without further purification. The multi-walled carbon nanotubes (MWCNTs, 10–15 nm outer diameter, 2–6 nm inner diameter and 0.1–10 μm length), 3-bromopropan-1-amine and triethanolamine were obtained from the Sigma–Aldrich (St. Louis, MO, USA). All the supplementary chemicals were of analytical grades and solutions were prepared with deionized water. The phosphate buffer solution (PBS) was prepared from phosphoric acid (H_3PO_4), potassium dihydrogen phosphate (KH_2PO_4) and dipotassium hydrogen phosphate (K_2HPO_4) and adjusting the pH was controlled with hydrochloric acid (HCl) and potassium hydroxide (KOH) solutions.

2.2. Apparatus and instrumentations

Autolab electrochemistry instruments (Autolab, Eco Chemie, Netherlands) was used for amperometry measurements and electrochemical impedance spectroscopy (EIS). Cyclic voltammetry (CV) measurements were carried out on a Metrohm (797 VA Computrace, Switzerland) controlled by a personal computer. A saturated calomel electrode (SCE) as reference electrode and a platinum wire as auxiliary electrode were used. Fourier transform infrared spectroscopy (FTIR) data were recorded on a Perkin Elmer GX FTIR spectrometer. The structure and the morphology of the samples were characterized using a digital scanning electron microscope (SEM) (Model KYKY-EM3200, KYKY, China) and a Hitachi HT-7100 (100 kV) transmission electron microscope (TEM). The magnetic properties were analyzed with vibrating sample magnetometer (VSM) (LDJ 9600-1, USA). X-ray diffraction (XRD) patterns were obtained on a powder X-ray diffraction system from PANalytical model X'Pert PRO (PANalytical B.V., Almelo, The Netherlands). A digital pH-meter (780 pH meter, Metrohm) with precision of ±0.001 was used to read the pH value of the buffer solutions. All experiments were performed at room temperature (25 ± 2 °C). Electrolyte solutions were deoxygenated by purging pure nitrogen (99.99%) for 10 min prior to electrochemical experiments.

2.3. Synthesis process

2.3.1. Preparation of the magnetic Fe_3O_4 nanoparticles

Magnetic iron oxide nanoparticles were synthesized according to a previous report [31]. In brief, $FeCl_3{\cdot}6H_2O$ (5.838 g, 0.0216 mol) and $FeCl_2{\cdot}4H_2O$ (2.147 g, 0.0108 mol) were dissolved in 100 mL deionized water at 85 °C under N_2 atmosphere and vigorous mechanical stirring (500 rpm). Then, 10 mL of 25% NH_4OH was quickly injected into the reaction mixture in one portion. The addition of the base to the Fe^{2+}/Fe^{3+} salt solution resulted in the formation of the black precipitate of Fe_3O_4 NPs immediately. The reaction continued for another 25 min and the mixture was cooled to room temperature. Subsequently, the resultant ultrafine magnetic particles were treated by magnetic separation and washed several times by deionized water.

2.3.2. Preparation of amine functionalized IL

The amine functionalized IL, 3-amino-*N,N,N*-tris(2-hydroxyethyl)propan-1-aminium bromide (amine-IL), was prepared by stirring 3-bromopropan-1-amine (1.0 mmol) and triethanolamine (1.0 mmol) in 5 mL methanol at room temper-

ature for 4 days. The mixture was washed with ethyl acetate to remove any unreacted reactants, followed by filtration to afford white precipitates of amine functionalized IL.

2.3.3. Preparation of amine-IL Modified MWCNTPreparation of amine-IL modified MWCNT

Pristine MWCNTs (p-MWCNTs) were refluxed under stirring in the mixture of 1:3 (v/v) HNO_3 and H_2SO_4 at 70 °C for 30 h, which was followed by centrifugation and repeated washings with DI water. The carboxylated MWCNTs (MWCNTs-COOH) thus obtained were dried at 60 °C for 1 day under reduced pressure and reacted with excess of $SOCl_2$ at room temperature for 24 h. The acylated MWCNTs (MWCNTs-COCl) were separated by centrifugation, subsequently washed with anhydrous THF to remove excess of $SOCl_2$, and dried in vacuum at 50 °C for 12 h. The final product was then subjected to functionalization with amine-IL. The obtained MWCNTs-COCl and amine-IL, in the optimum ratio 5:1 w/w, were mixed with 50 mL solution of DMF and TEA (1 mL) and then stirred at 120 °C for 2 days. The thus obtained solid MWCNT-IL was separated by filtration and washed with ethanol for three times, followed by drying in a vacuum.

2.3.4. Preparation of MWCNT-IL-Fe_3O_4 nanocomposite

MWCNT-IL-Fe_3O_4 nanocomposite was prepared as follows: 100 mg of the synthesized Fe_3O_4 NPs were dispersed in 20 mL of H_2O and the resultant suspension was added dropwise into 500 mg of MWCNT-IL that was initially dispersed in 50 mL DI water by sonication. The mixture was stirred and sonicated vigorously for 30 min. Finally, suspension stirred with a mechanical stirrer for 24 h at room temperature. After this time, the MWCNT-IL-Fe_3O_4 nanocomposite was separated by a magnet and washed by ethanol, H_2O and acetone respectively to remove the unattached substrates and dried in vacuum at 40 °C for 24 h. Scheme 1A depicted the synthetic procedure of MWCNT-IL-Fe_3O_4nanocomposite.

2.4. Design and fabrication of Ag@MWCNT-IL-Fe_3O_4 nanocomposite and GOx modified biosensor

At the first step, the MGCE was prepared according to Peng report [35]. Briefly a homogeneous paste was fabricated by the addition of paraffin oil into the graphite powder. A portion of the carbon paste was put into one end of a Teflon tube and a nummular magnet (2 mm in thickness, 3 mm in diameter and 0.2 T at the surface) was inserted with a depth of 2 mm from the surface of electrode. The electrical contact was established by a copper wire that inserted through the opposite end of Teflon tube. At final a glassy carbon (3 mm in diameter and 2 mm in depth) was inserted in the tube to impede the magnet and the edge of the glassy carbon was fixed by the adhesive. The prepared MGCE surface was smoothed on a piece of weighing paper with alumina slurry, rinsed thoroughly with water and sonicated in deionized water.

At the second step, the clean MGCE was immersed into 0.1 mL of 1 mg mL^{-1} MWCNT-IL-Fe_3O_4 aqueous suspension to firmly attachment of MWCNT-IL-Fe_3O_4 NPs onto the MGCE surface due to the magnetic force. Subsequently, the MWCNT-IL-Fe_3O_4/MGC electrode was rinsed with deionized water and dried in the air. The MWCNT-IL-Fe_3O_4/MGC electrode was immersed into the 1.0 mM $AgNO_3$ solution containing 0.1 M KNO_3, which was earlier deaerated by bubbling with nitrogen, and the electrochemical deposition was conducted at 0.0 V for 180 s [36]. Then, the AgNPs decorated MWCNT-IL-Fe_3O_4/MGC electrode, which was denoted as Ag@MWCNT-IL-Fe_3O_4/MGCE, was washed with deionized distilled water and dried under a stream of nitrogen. The GOx/Ag@MWCNT-IL-Fe_3O_4/MGCE was prepared by dropping 6 μL of 2.0 mg mL^{-1} GOx in 0.1 M PBS of pH 5 on to the Ag@MWCNT-IL-Fe_3O_4/MGCE. Afterwards drying at 4 °C in a refrigerator for 5 h, 6 μL of glutaraldehyde solution, (2.5%, w/v), was casted and the final modified biosensor dried at 4 °C. Scheme 1B illustrates the schematic design of the proposed GOx biosensor. For comparison, the GOx/MWCNT-IL-Fe_3O_4/MGCE and GOx/MGCE was also prepared according to the same procedure. All the GOx-immobilized electrodes were stored at 4 °C when not in use.

3. Results and discussion

3.1. Characterization of MWCNT-IL-Fe_3O_4 nanocomposite

The sequential coating of IL and Fe_3O_4 NPs on the MWCNTs was confirmed using FTIR spectroscopy. Fig. 1A shows the FTIR spectra obtained for p-MWCNTs (a), MWCNTs-COOH (b), MWCNTs-COCl (c), MWCNT-IL (d) and MWCNT-IL-Fe_3O_4 (e). Comparison of the FTIR spectra of MWCNTs-COOH with p-MWCNTs, as it is seen in the curve b, the band at 1723 cm^{-1} is corresponding to carbonyl stretch of the carboxylic acid group. The converting of the carboxylic acid groups (MWCNTs-COOH) into the acyl chloride intermediate (MWCNTs-COCl) by treatment with thionyl chloride was confirmed by the appearance of peak near 1775 cm^{-1} strechning in curve c. Curve d shows the spectrum of MWCNT-IL and the absorption band at 1655 cm^{-1} was attributed to the carbonyl stretching of the amide groups (-CONH-). Also, the bands observed around 2953 cm^{-1} were assigned to the bending vibration of CH_2. The prominent IR bands at 3300 and 1579 cm^{-1} were ascribed to the NH and OH stretching vibrations. These results indicated that the amine-IL was bonded to the surface of MWCNTs through amidation reaction. Curve e shows the spectrum of MWCNT-IL-Fe_3O_4 and the appearance absorption bands at 624 and 572 cm^{-1} are attributed to the vibrations of Fe-O bonds of iron oxide. Generally, the peaks at Fig. 1e displayed the successful attachment of amine-IL and Fe_3O_4 NPs on the surface of MWCNTs.

The magnetic property of as-prepared Fe_3O_4 and MWCNT-IL-Fe_3O_4 were measured by VSM method at room temperature. Fig. 1B shows the magnetization–hysteresis loops of samples with different composition. The magnetic saturation (Ms) for Fe_3O_4 was 65.4 emu g^{-1}, and that of MWCNT-IL-Fe_3O_4 was 45.2 emu g^{-1}. This decrease in Ms can be attributed to the interaction of MWCNT-IL and the Fe_3O_4 NPs, which will reduce the magnetic moment. Significantly, the results indicate that the obtained MWCNT-IL-Fe_3O_4 possess strong magnetization and superparamagnetism, which are advantageous to the fabrication of the biosensor based on a magnetic glassy carbon electrode.

The XRD patterns of Fe_3O_4 NPs, MWCNT-IL and MWCNT-IL-Fe_3O_4 composite are shown in Fig. S-1. The diffraction peaks at values of 30.42°, 35.76°, 43.33°, 53.80°, 57.37° and 62.98° can be indexed respectively to the (220), (311), (400), (422), (511) and (440) planes of the magnetite nanoparticles with a spinel structure (JCPDS Card No. 19-0629) [37]. On the contrary, the diffraction peak at $2\theta = 26.2°$ corresponds to 002 planes of MWCNTs, which was observed for both MWCNT-IL and MWCNT-IL-Fe_3O_4 nanocomposite. Based on the XRD patterns, it can be concluded that the Fe_3O_4 NPs are well covered on the MWCNT-IL surface.

3.2. Characterization of Ag@MWCNT-IL-Fe_3O_4 nanocomposite

The morphology and structure of the as-prepared Ag@MWCNT-IL-Fe_3O_4 nanocomposite were characterized by TEM and SEM, and some representative images are shown in Fig. 2. Highly porous 3D structured Ag@MWCNT-IL-Fe_3O_4 nanocomposite can be seen from SEM image (Fig. 2A). MWCNTs can be considered as the framework and both the Ag NPs and Fe_3O_4 NPs are grown along them. The energy dispersive x-ray spectrometer (EDS) measurement of the Ag@MWCNT-IL-Fe_3O_4 composite presents signals of

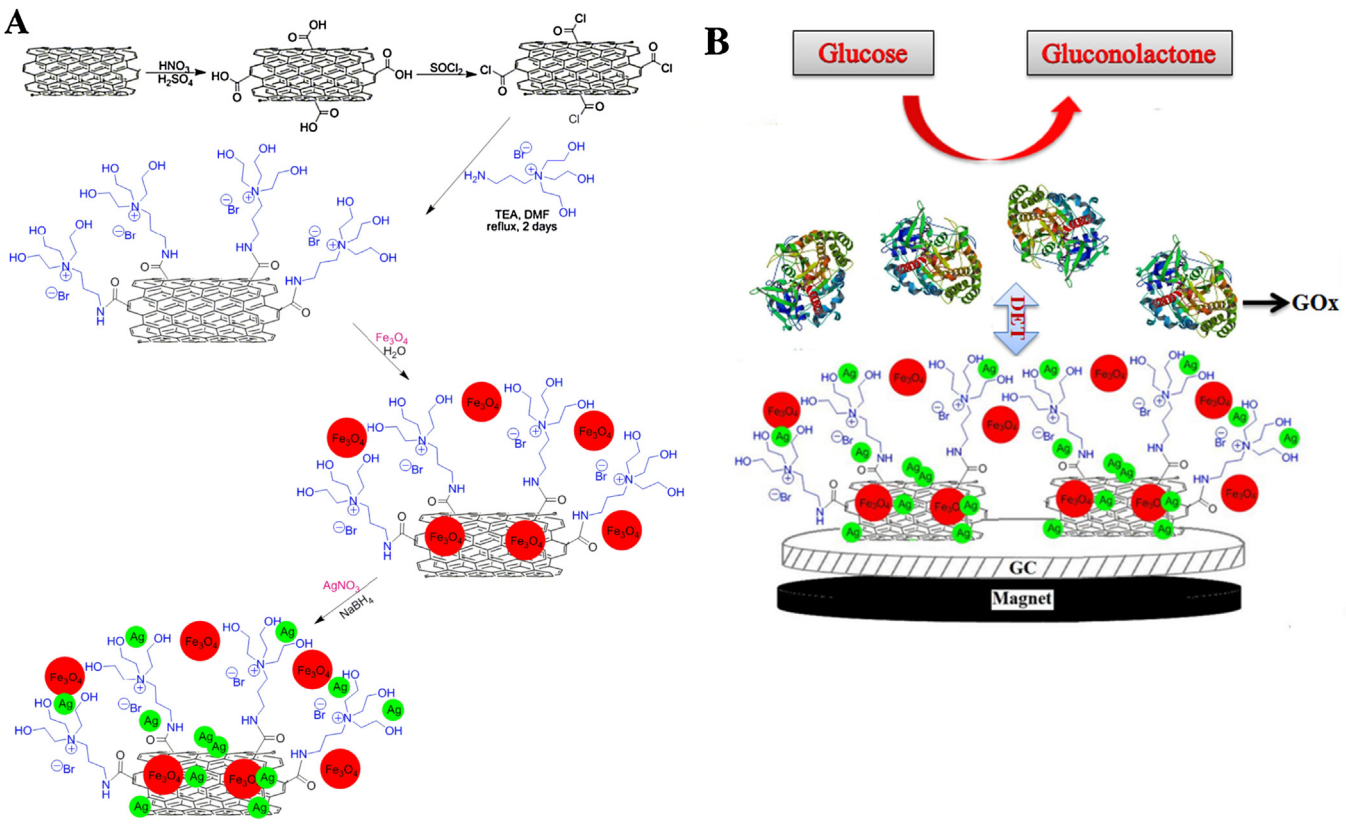

Scheme 1. (A) Demonstration route for preparation of Ag@MWCNT-IL-Fe_3O_4 nanocomposite. (B) Schematic illustration for the DET from GOx to MGCE at fabricated biosensor.

carbon, nitrogen, oxygen, iron and silver elements with weight percentages of 34.87%, 6.63%, 13.11%, 24.56% and 20.83%, respectively (inset at Fig. 2A), approving the successful formation of the prepared nanocomposite. In combination with SEM, the elemental EDS mapping characterization was applied to study the chemical composition and elemental distribution in Ag@MWCNT-IL-Fe_3O_4 nanocomposite. Fig. 2B collects representative SEM image and corresponding EDS spectrum for the synthesized nanocomposite. As can be seen, typical EDS elemental mapping of elements shows that C, Fe, and Ag are homogeneously distributed in the Ag@MWCNT-IL-Fe_3O_4 nanocomposite. Fig. 2C shows the TEM images of the Ag@MWCNT-IL-Fe_3O_4 nanocomposite. As shown in Fig. 2C (a), the Ag NPs and Fe_3O_4 NPs are distributed uniformly on the MWCNTs, and the nanoparticles are mainly without aggregation. The prepared NPs are evenly sized in the range from 10 to 15 nm. Well-dispersed nanoparticles on walls and ends of the MWCNTs is apparent at TEM image with high magnification (Fig. 2C (b)).

The formation of Ag NPs on the MWCNT-IL-Fe_3O_4 surface was evaluated using electrochemical measurements. Fig. 3A shows CV voltammograms of Ag@MWCNT-IL-Fe_3O_4/MGCE (curve b) and a blank MWCNT-IL-Fe_3O_4/MGCE (curve a) in N_2 saturated 0.1 M PBS (pH 7.0) at the potential range −0.15 to +0.27 V. From the results, neither reduction nor oxidation peak were observed on MWCNT-IL-Fe_3O_4 electrode. In contrast, Ag@MWCNT-IL-Fe_3O_4 electrode showed a clear anodic and cathodic peak current which appeared at 0.15 V and −0.02 V, respectively, reflecting the redox behavior of metallic Ag [38]. Therefore, the redox peaks of curve b in Fig. 3A also prove the presence of Ag NPs on the surface of Ag@MWCNT-IL-Fe_3O_4.

The conformational integrity of immobilized GOx on the Ag@MWCNT-IL-Fe_3O_4 nanocomposite is critical in the following investigation of its direct electrochemistry and electrocatalytic properties. Therefore, FTIR spectra of Ag@MWCNT-IL-Fe_3O_4 nanocomposite (curve a) pure GOx (curve b) and the GOx/Ag@MWCNT-IL-Fe_3O_4 (curve c) were studied and offered in Fig. 3B. In the FTIR spectrum of GOx (curve b), the intense absorption peak appearing at the wavenumber of 3410 cm^{-1} is assigned for N—H stretching. Also, two peaks centered at 1640 and 1525 cm^{-1} are assigned to the characteristic amide I and II absorption bands of GOx. The peak appearing around 1101 cm^{-1} was assigned to the stretching vibration of C—O of enzyme [39]. Disappearance of the amide II band at immobilized GOx is one of reasons for denaturation and unfolding of the enzyme [40]. However, the FTIR spectra of GOx/Ag@MWCNT-IL-Fe_3O_4 (curve c), as same as those of native GOx, presents absorption bands of the amide I (1647 cm^{-1}) and II (1532 cm^{-1}) suggesting an unchanged native structure for the immobilized GOx. The slight shifts of amide I and II absorption bands can be attributed to hydrophobic interactions between GOx and Ag@MWCNT-IL-Fe_3O_4 nanocomposite.

3.3. Direct electrochemistry of GOx/Ag@MWCNT-IL-Fe_3O_4/MGCE

GOx, as one of most studied flavoenzymes, is identified by redox activity of deeply buried flavin adenine dinucleotide (FAD) center. This center is reduced by glucose to 1,5-dihydro-FAD ($FADH_2$). In actual, a two-electron two-proton redox reaction as $FAD + 2H^+ + 2e^- \leftrightarrow FADH_2$ forms the base of the electrochemical glucose biosensors. If the $FADH_2$ can be oxidized back to FAD, resulting in the turning over of GOx without employment of oxygen or other electrochemical mediators, the process is called as bioelectrocatalysis or direct electron transfer (DET) of GOx. As shown in Fig. 4A, in an oxygen-free solution, while no redox peaks were observed at, GOx/MGCE (curve a), there was a pair of well-defined reversible redox peaks at the GOx/MWCNT-

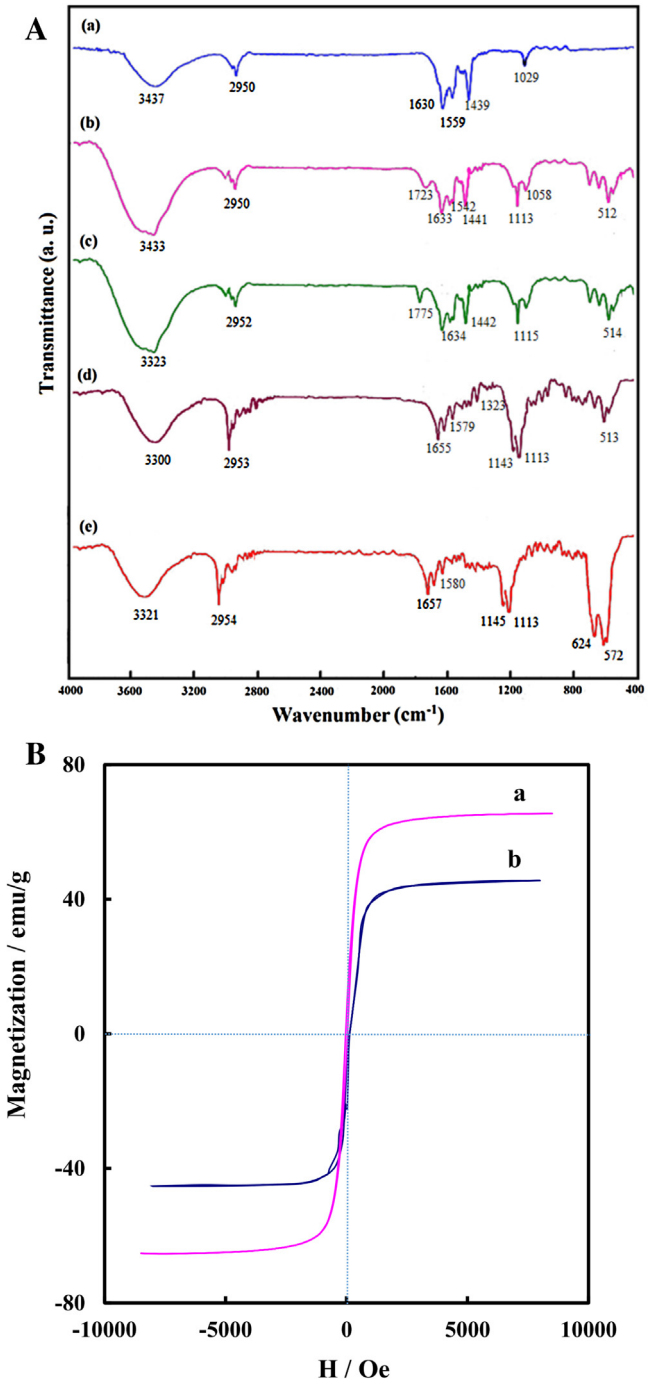

Fig. 1. (A) FTIR spectra of p-MWCNTs (a), MWCNTs-COOH (b), MWCNTs-COCl (c), MWCNTs-IL (d) and MWCNT-IL-Fe_3O_4 (e). (B) Magnetization curve of Fe_3O_4 NPs (a) and MWCNT-IL-Fe_3O_4 (b).

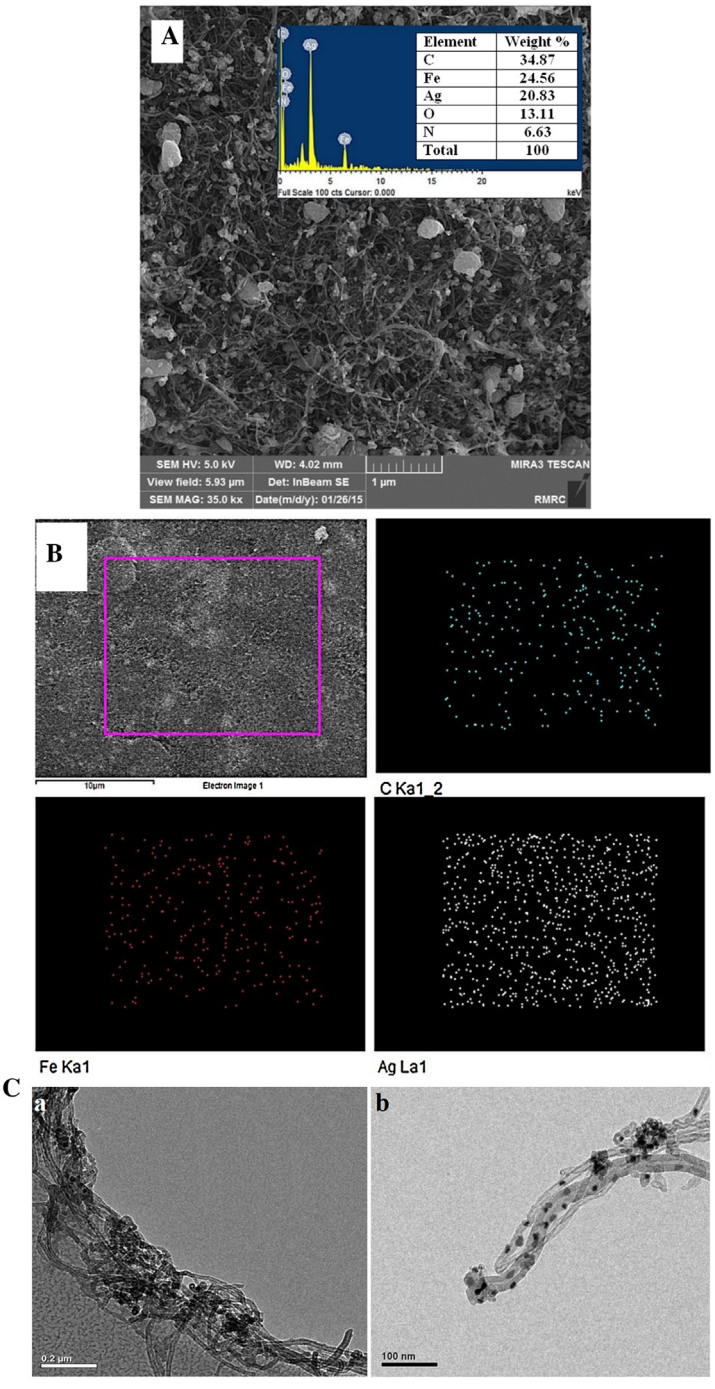

Fig. 2. (A) SEM image of Ag@MWCNT-IL-Fe_3O_4 nanocomposite. Inset: EDS measurement of the Ag@MWCNT-IL-Fe_3O_4. (B) Elemental EDS mapping characterization of Ag@MWCNT-IL-Fe_3O_4 nanocomposite. (C) Typical TEM image of Ag@MWCNT-IL-Fe_3O_4 nanocomposite (curve a), TEM image with high magnification of Ag@MWCNT-IL-Fe_3O_4 nanocomposite (curve b).

IL-Fe_3O_4/MGCE (curve b) and GOx/Ag@MWCNT-IL-Fe_3O_4/MGCE (curve c). The obtained formal potential for GOx/MWCNT-IL-Fe_3O_4/MGCE and GOx/Ag@MWCNT-IL-Fe_3O_4/MGCE (defined as half of sum of anodic and cathodic peak potential, $E^{\circ\prime}$) were −0.46 V and −0.44 V (vs. SCE), respectively, which were close to the reported standard electrode potential of GOx [41]. This clearly shows that both MWCNT-IL-Fe_3O_4 and Ag NPs-containing nanocomposite (Ag@MWCNT-IL-Fe_3O_4) can play an important role in the GOx adsorption. However, in the absence of Ag NPs, the current response at GOx/MWCNT-IL-Fe_3O_4/MGCE is 1.4 times smaller than that of the GOx/Ag@MWCNT-IL-Fe_3O_4/MGCE. This result indicates that the presence of Ag NPs the surface of GOx/Ag@MWCNT-IL-Fe_3O_4 has a great advantage in the DET with GOx compared to GOx/MWCNT-IL-Fe_3O_4 and might play an important role in the appropriate GOx orientation and construct a biocompatible and conductive microenvironment which promotes DET between GOx and GC electrode [42]. As the direct electrochemistry of GOx is due to the redox reaction of FAD, where two protons and two electrons are exchanged, the effect of different pH solutions on peak potentials was investigated for GOx/Ag@MWCNT-IL-Fe_3O_4/MGCE. Fig. S-2 of the Supporting information shows cyclic voltammograms of GOx/Ag@MWCNT-IL-Fe_3O_4/MGCE in 0.1 M PBS with

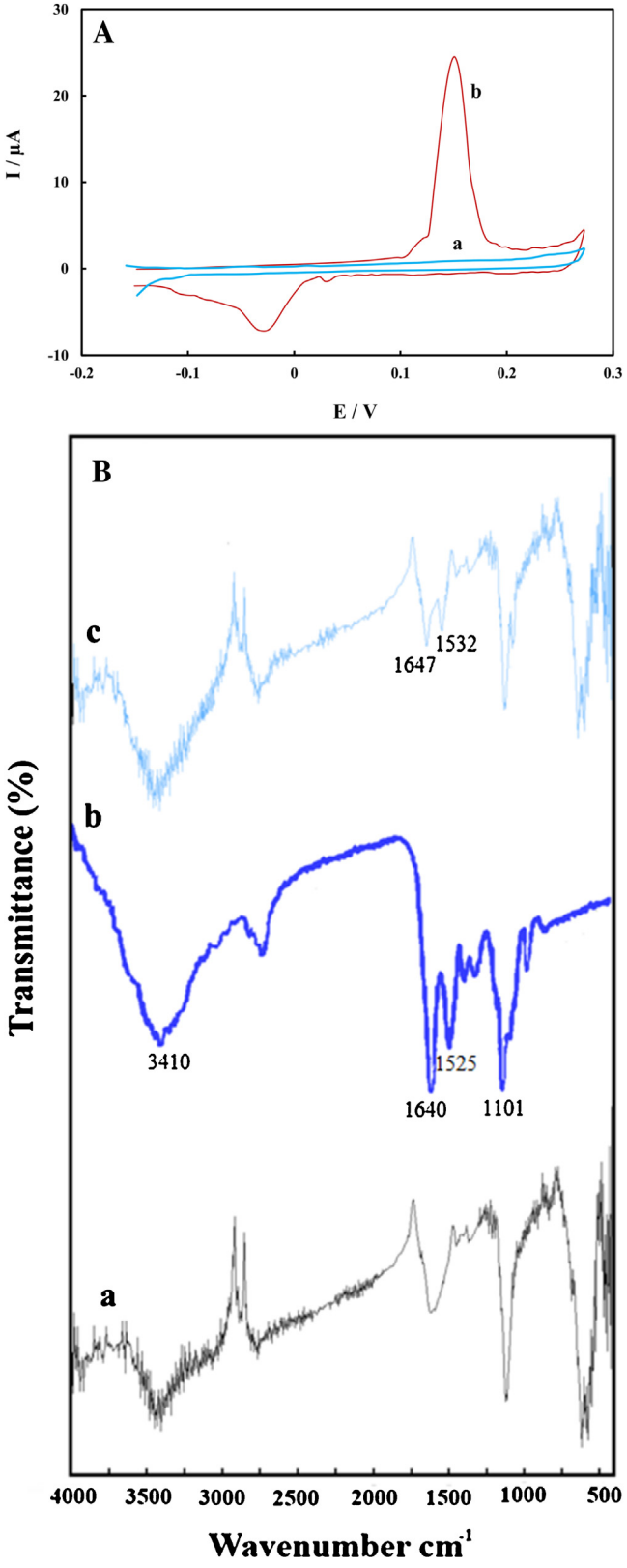

Fig. 3. (A) CVs of MWCNT-IL-Fe_3O_4/MGCE (curve a) and Ag@MWCNT-IL-Fe_3O_4/MGCE (curve b) in 0.1 M pH 7.0 PBS. (B) FT-IR spectra of Ag@MWCNT-IL-Fe_3O_4 (curve a), pure GOx (curve b), and GOx/Ag@MWCNT-IL-Fe_3O_4 (curve c).

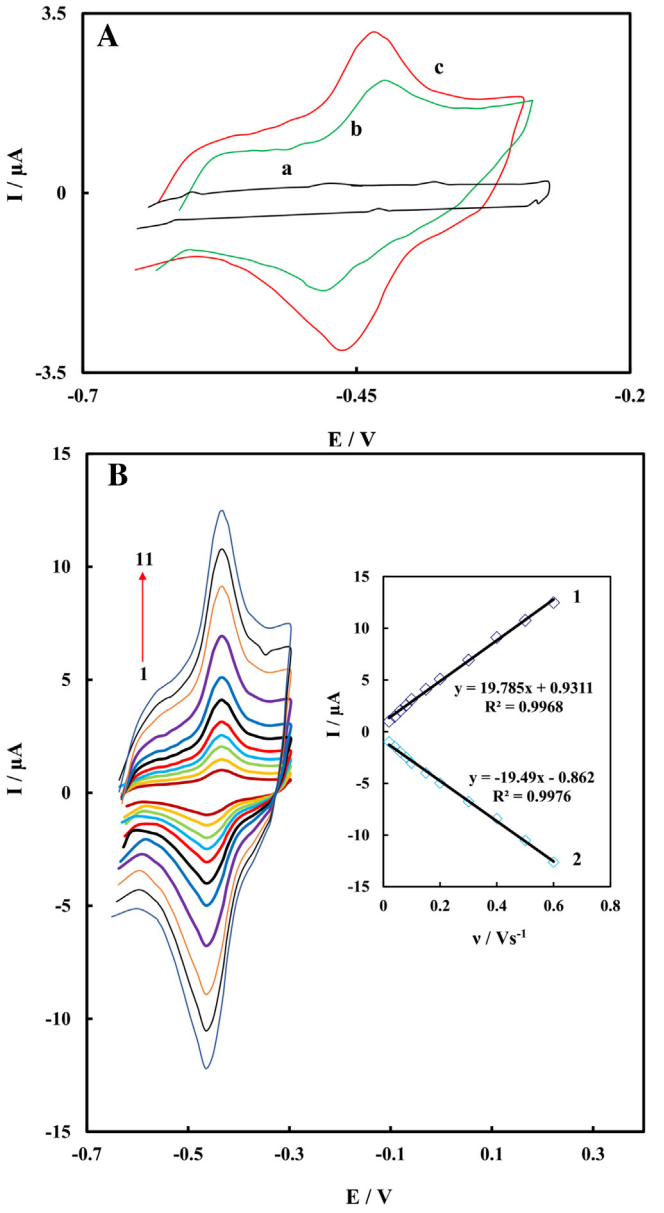

Fig. 4. (A) Cyclic voltammograms of the GOx-GCE (a), GOx/MWCNT-IL-Fe_3O_4/MGCE (b), GOx/Ag@MWCNT-IL-Fe_3O_4/MGCE (c) in N_2-saturated 0.1 M pH 7.0 PBS at scan rate of 0.1 V s^{-1}. (B) Cyclic voltammograms of GOx/Ag@MWCNT-IL-Fe_3O_4/MGCE in 0.1 M PBS (pH 7.0) at different scan rates of (1) 0.02, (2) 0.04, (3) 0.06, (4) 0.08, (5) 0.1, (6) 0.15, (7) 0.2, (8) 0.3, (9) 0.4, (10) 0.5 and (11) 0.6 V s^{-1}. Inset a: Plot of the anodic (1) and cathodic (2) peak current against the scan rate.

different pH values. As can be seen, the observed stable and well-defined redox peaks exhibited a negative shift with increasing pH values from 4.0 to 9.0. The obtained formal potential exhibits linear relationship with solution pH with a slope of −56.1 mV/pH which is close to reported theoretical value of −58.6 mV/pH for a reversible two proton and two electron transfer reaction [39].

Valuable information about electrochemical mechanism usually can be attained from the study of an electrochemical redox reaction at different scan rates. Fig. 4B shows an overlap of cyclic voltammograms of GOx in deoxygenated buffer with different scan rates from 0.02–0.6 V s^{-1}. As shown at inset a of Fig. 4B, the both anodic (I_{pa}) and cathodic (I_{pc}) peak currents exhibit a linear relationship with variation at scan rates. Also, the consumed charges, Q (attained from integrating the anodic or cathodic peak area), is

constant at cyclic voltammograms with subtracted background. Moreover, ratio of the slopes (S_{Ipc}/S_{Ipa}) for plots of I_{pc} vs. ν and I_{pa} vs. ν was close to 1 at the studied potential scan rates. These results propose that the electrochemical reaction of FAD center at the immobilized GOx on the surface of the Ag@MWCNT-IL-Fe_3O_4 is a quasi-reversible and surface-controlled thin-layer electrochemical reaction. On the other word, in this process all electroactive FAD centers of enzyme [GOx-FAD], produced by the oxidation of $FADH_2$ centers [GOx-$FADH_2$] on the anodic scan, could be reduced to $FADH_2$ on the cathodic scan. In this situation, the surface coverage concentration of the electroactive GOx (Γ^*) can be considered by integrating the CV cathodic peak and applying the equation of $Q = nFA\Gamma^*$, where Q is the integrated charge (C) of the cathodic peak and the charge value (Q) is almost constant at various potential scan rates, A is the electrode area, and n is the number of involved electrons. In the range of scan rate from 0.02–0.6 V s^{-1}, the average Γ^* value was 5.84×10^{-11} mol cm^{-2}. This value is about 20 times higher than the theoretical value of 2.86×10^{-12} mol cm^{-2} for monolayer GOx on bare GCE [42]. This demonstrates that the Ag@MWCNT-IL-Fe_3O_4 nanocomposite has provided high surface area for DET reaction of GOx.

According Laviron method, for diffusionless CVs, the apparent heterogeneous electron transfer rate constant (k_s) can be calculated when the potential separation of redox peak is less than 200 mV using below equation:

$$\log k_s = \alpha \log(1-\alpha) + (1-\alpha)\log\alpha - \log(RT/nF\upsilon) - (1-\alpha)\alpha F\Delta E_p/2.3RT \quad (1)$$

where α is charge transfer coefficient which is 0.5 and other parameters representing their usual meanings. In this study, at $\nu = 0.1$ V s^{-1} and $\Delta E_p = 0.034$ V, the k_s value was calculated to be 4.65 (±0.04) s^{-1}, which is larger than the value observed for the GOx at grapheme-chitosan modified electrode (2.83 s^{-1}) [43], gold nanoparticles decorated graphene-carbon nanotubes (3.36 s^{-1}) [44], gelatin-multiwalled carbon nanotube (1.08 s^{-1}) [45], the graphene and cobalt phthalocyanine composite (3.57 s^{-1}) [46] and poly(2,6-diaminopyridine)/carbon nanotube electrode (4.0 s^{-1}) [47] exposing that the DET rate of immobilized GOx on Ag@MWCNT-IL-Fe_3O_4 nanocomposite is acceptable.

3.4. Electrocatalytic activity of GOx/Ag@MWCNT-IL-Fe_3O_4/MGCE at glucose detection

Electrocatalytic activity of GOx/Ag@MWCNT-IL-Fe_3O_4/MGCE was investigated using cyclic voltammetry in N_2 (curve a) and air (curve b) saturated PBS at the scan rate of 100 mV s^{-1} (Fig. 5A). As expected, under deaerated condition, a pair of well-defined redox peaks devised from the reversible reaction of FAD/$FADH_2$ was observed (curve a). Different from the obtained CVs in deaerated solution, the biosensor showed a sharp increase in the reduction current in aerated PBS without glucose (curve b). In this situation, the large cathodic current observed at GOx/Ag@MWCNT-IL-Fe_3O_4/MGCE can be attributed to dissolved oxygen reduction, as a natural co-substrate for GOx, which is electrochemically catalyzed by the reduced GOx ($FADH_2$):

$$\text{GOx-FAD} + 2e^- + 2H^+ \leftrightarrow \text{GOx-FADH}_2 \quad (2)$$

$$\text{GOD-FADH}_2 + O_2 \rightarrow \text{GOx-FAD} + H_2O_2 \quad (3)$$

In the air saturated PBS when glucose is added (Fig. 5B), the reduction peak current decreased indicating the enzymatic reaction (Eqs. (3) and (4)) increased consumption of oxygen and limited the electrochemical reaction (Eq. (2)) at the electrode surface.

$$\text{GOx-FAD} + \text{Glucose} \rightarrow \text{GOx-FADH}_2 + \text{Gluconolactone} \quad (4)$$

According to above results, decline at electrocatalytic currents after the decrease of dissolved oxygen, the proposed biosensor can be employed to electrocatalytic sense of glucose in oxygenated biological system.

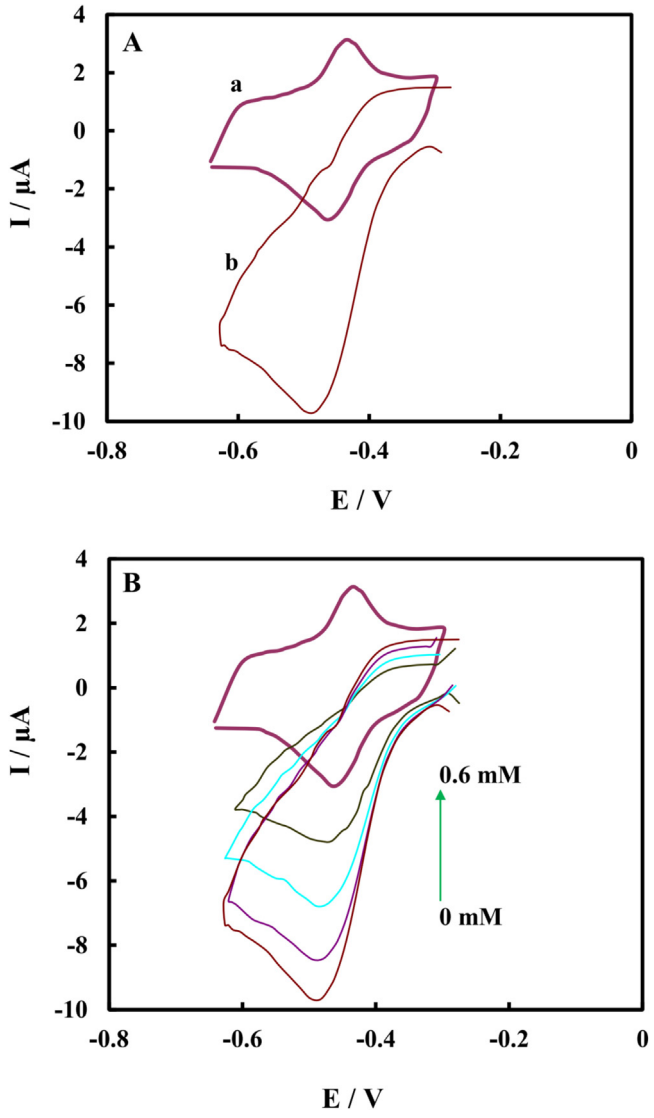

Fig. 5. (A) Cyclic voltammograms of GOx/Ag@MWCNT-IL-Fe_3O_4/MGCE operated in (a) N_2-saturated and (b) air saturated, 0.1 M, pH 7.0 PBS. (B) Cyclic voltammograms of GOx/Ag@MWCNT-IL-Fe_3O_4/MGCE operated in air saturated PBS at increasing glucose concentration (0, 0.2, 0.4 and 0.6 mM). Scan rate: 0.1 V s^{-1}.

3.5. Analytical performance of GOx/Ag@MWCNT-IL-Fe_3O_4

Fig. 6 displays the amperometric responses of biosensor for various concentration of glucose. Aliquots of glucose were injected at 20 s regular intervals into continuously stirred air saturated PBS (pH 7.0). The applied electrode potential was hold at −0.51 V. Rapid and well defined responses were observed for each addition. The result shows the response time of the biosensor toward glucose is quick and reaches to a stable plateau less than 5 s. The linear response range of the biosensor to glucose concentration is in the range from 6 μM to 2.0 mM (inset of Fig. 6). The detection limit is estimated to be 2.12 μM (based on S/N = 3) which is comparable with or, in most cases, lower than the other GOx modified electrodes [42–51] (see Table 1). These results indicate that GOx at proposed biosensor has appropriate bioelectrocatalytic activity toward glucose detection.

As shown in the inset a of Fig. 6, when the amount of added glucose is increased to a confident concentration (2.0 mM at

Table 1
Comparison of the analytical performance of the proposed electrode with other glucose biosensors.

Modified electrode	Electrode type	K_s (s^{-1})	Linear range (mM)	Detection limit (mM)	Ref.
GOx/Graphene oxide-carbon nanotube hybrid	GCE	9.0	2–8	0.5	[42]
GOx/Graphene-chitosan nanocomposite	GCE	2.83	0.08–12	0.02	[43]
GOx/Gold nanoparticles decorated graphene-carbon nanotubes	GCE	3.36	0.01–2 2–5.2	0.0041 0.95	[44]
GOx/Gelatin-multiwalled carbon nanotube	GCE	1.08	6.30–20.09	–	[45]
GOx/Graphene and cobalt phthalocyanine composite	GCE	3.57	0.01–14.8	0.0016	[46]
GOx/Poly(2,6-diaminopyridine)-carbon nanotube electrode	GCE	4	0.00042–8.0	0.00013	[47]
GOx/Manganese dioxide particles-decorated reduced graphene oxide sheets	GCE	4.92	0.04–10	0.02	[48]
GOx/Reduced graphene oxide and silver nanoparticles	GCE	5.27	0.5–12.5	0.16	[49]
GOx/Graphene-polyaniline-gold nanoparticles	SPCE[a]	–	0.2–11.2	0.1	[50]
GOx/Polyaniline-poly(acrylic acid) composite	Gold film	–	–	0.06	[51]
GOx/Ag@MWCNT-IL-Fe_3O_4	MGCE	4.65	0.006–2.0	0.00212	This work

[a] Screen-printed carbon electrode.

Table 2
Results of the glucose detection and the recovery test for real sample analysis (n = 5).

Sample	Added (μM)	Found (μM)	R.S.D	Recovery (%)	Determined by titration method	R.S.D
A	0	–	–	–	–	–
	30	28.8 ± 0.06	2.9	96	29.2 ± 0.06	2.1
	50	49.2 ± 0.03	2.3	98.4	50.1 ± 0.04	1.7
B	0	–	–	–	–	–
	200	201.1 ± 0.04	2.6	100.5	201.1 ± 0.04	3.3
	600	599.4 ± 0.07	2.6	99.9	600.4 ± 0.05	2.8
C	0	78.6 ± 0.05	3.1	–	78.2 ± 0.04	1.9
	100	178.5 ± 0.06	2.5	99.9	178.7 ± 0.05	2.1
	150	228.9 ± 0.04	2.2	100.1	228.2 ± 0.04	2.2
D	0	932.0 ± 0.04	1.5	–	931.1 ± 0.06	2.1
	50	981.4 ± 0.05	2.8	99.9	982.6 ± 0.04	2.7
	200	1130.2 ± 0.07	2.1	99.8	1131.4 ± 0.05	2.3

A and B samples of glucose in urine samples (male, healthy volunteers).
C and D samples of glucose in rain samples (male, diabetic volunteers).

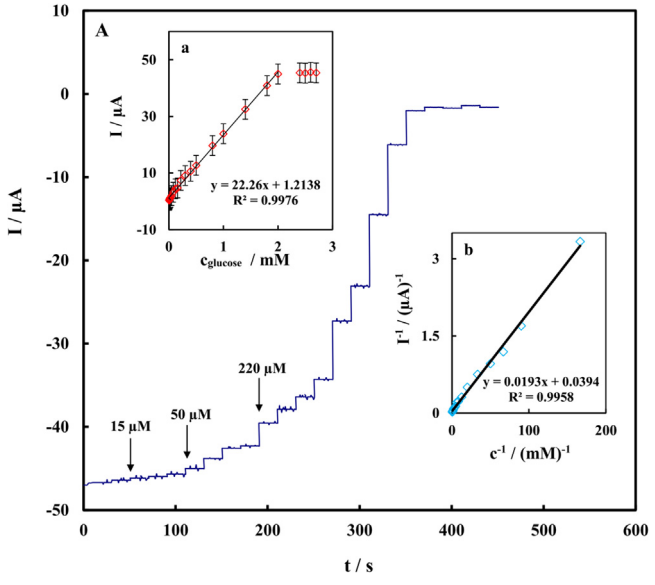

Fig. 6. The amperometric response of the biosensor to successive addition of different concentration of glucose in air saturated PBS (pH 7.0) at the working potential of −0.51 V. Inset a: plot of amperometric response current vs. glucose concentration ($c_{glucose}$). Inset b: plot of the reciprocal of steady-state current (I_{ss}) versus the reciprocal of glucose concentration for the GOx/Ag@MWCNT-IL-Fe_3O_4/MGCE.

here), catalytic current turns from linearity to a platform, showing the Michaelis-Menten kinetic mechanism for biological activity reaction of immobilized enzyme [39]. On the basis of the Lineweaver-Burk equation in electrochemical format and related plot (inset b of Fig. 6A) [31], the apparent Michaelis-Menten constant (K_M^{app}) was calculated to be 0.49 mM. The obtained value for K_M^{app} is much smaller than the value of 0.76 mM for GOx immobilized on graphene quantum dots [52], 0.6 mM for GOx immobilized on Graphene/polyaniline/gold nanoparticles nanocomposite [53], 2.95 mM for GOx immobilized on onto glassy carbon electrode modified with nitrophenyl diazonium salt [54] and 5.20 mM for GOx immobilized on glassy carbon electrode modified with gold–platinum alloy nanoparticles/multiwall carbon nanotubes [55]. The smaller value of K_M^{app} proposes that the immobilized GOx on the Ag@MWCNT-IL-Fe_3O_4 retains higher enzymatic activity and can exhibit high affinity for glucose detection.

Storage stability of the biosensor, stored at 4 °C in refrigerator, was determined by monitoring the variation in its current response to 0.4 mM glucose. The current response of the biosensor was found to be properly constant during the first investigation week, and then to drop slowly with time. After two weeks, the current retained more than 93% in comparison with primary response. After four weeks, there was a decrease of 21% from the primary current response. The decreased sensitivity may be attributed to the decline in enzyme activity [56]. The reusability of the biosensor was also studied by using the one same electrode for 10 successive determination of 0.4 mM glucose in the air saturated PBS (pH 7.0) and a satisfactory RSD value of 3.4% for 10 successive runs was obtained. The fabrication reproducibility of three biosensor, prepared at same way independently, was also studied in 0.4 mM glucose. An acceptable reproducibility with a RSD value of 5.1% was obtained. These results prove the proper stability of immobilized GOx on Ag@MWCNT-IL-Fe_3O_4 nanocomposite, which made it a good candidate in the determination of glucose.

3.6. Selectivity and real sample analysis

Evaluation of the selectivity of biosensor is very important for analytical purposes. Selectivity of the GOx/Ag@MWCNT-IL-Fe_3O_4/MGCE was investigated using acetic acid, ethanol, ascorbic acid, uric acid and dopamine as interfering substances. Fig. S-3 of the Supporting information displays the amperometric responses obtained at the biosensor for sequential addition of 1200.0 μM mentioned interfering substances at regular intervals (10 s once) into air saturated PBS (after twice addition of 400.0 μM glucose). As shown in Fig. S-3, the responses for measuring of glucose do not show significant changes for each 3-fold excessive addition. These results confirm high selectivity of proposed biosensor toward glucose detection and make it proper for practical applications at real samples.

The developed biosensor was tested for its efficacy for the determinations of glucose in the real urine samples collected from a local laboratory without any sample treatment. The analysis was carried out using the standard addition method and results were compared with those achieved by a spectrophotometric method in a standard clinical laboratory. The obtained results are summarized in Table 2. It is clear from the data that there are good agreements between two different studied methods, indicating the proposed biosensor has practical application for glucose detection in real samples.

4. Conclusions

A novel magnetic nanocomposite, was synthesized, functionalized by Ag nanoparticles (Ag@MWCNT-IL-Fe_3O_4), and applied to immobilize GOx for DET reactions. The proposed glucose biosensor can be prepared by a rapid procedure onto a MGCE. The biosensor has demonstrated high sensitivity, stability, fast-responding time and a broad dynamic range. It has advantage for working at aerated environments. These results indicated that the proposed biosensor can be useful for the fabrication of the operative third generation biosensors and bioelectronics devices.

Acknowledgement

The authors would like to thank Hakim Sabzevari University Research Council for financial support of this research.

Appendix A. Supplementary data

Supplementary data associated with this article can be found, in the online version, at http://dx.doi.org/10.1016/j.snb.2017.04.100.

References

[1] J.E. Shaw, R.A. Sicree, P.Z. Zimmet, Global estimates of the prevalence of diabetes for 2010 and 2030, Diabetes Res. Clin. Pract. 87 (2010) 4–14.
[2] D. Zheng, S.K. Vashist, K. Al-Rubeaan, J.H. Luong, F.S. Sheu, Rapid and simple preparation of a reagentless glucose electrochemical biosensor, Analyst 137 (2012) 3800–3805.
[3] F. Tasca, M.N. Zafar, W. Harreither, G. Noll, R. Ludwig, L. Gorton, A third generation glucose biosensor based on cellobiose dehydrogenase from Corynascus thermophilus and single-walled carbon nanotubes, Analyst 136 (2011) 2033–2036.
[4] T. Noll, G. Noll, Strategies for wiring redox-active proteins to electrodes and applications in biosensors, biofuel cells, and nanotechnology, Chem. Soc. Rev. 40 (2011) 3564–3576.
[5] S. Pakapongpan, R.P. Poo-arporn, Self-assembly of glucose oxidase on reduced graphene oxide-magnetic nanoparticles nanocomposite-based direct electrochemistry for reagentless glucose biosensor, Mater. Sci. Eng. C 76 (2017) 398–405 (in press).
[6] C. Cai, J. Chen, Direct electron transfer of glucose oxidase promoted by carbon nanotubes, Anal. Biochem. 332 (2004) 75–83.
[7] J. Wang, Electrochemical glucose biosensors, Chem. Rev. 108 (2008) 814–825.
[8] L. Gorton, A. Lindgren, T. Larsson, F.D. Munteanu, T. Ruzgas, I. Gazaryan, Direct electron transfer between heme-containing enzymes and electrodes as basis for third generation biosensors, Anal. Chim. Acta 400 (1999) 91–108.
[9] W. Putzbach, N. Ronkainen, Immobilization techniques in the fabrication of nanomaterial-based electrochemical biosensors: a review, Sensors 13 (2013) 4811.
[10] O. Courjean, F. Gao, N. Mano, Deglycosylation of glucose oxidase for direct and efficient glucose electrooxidation on a glassy carbon electrode, Angew. Chem. Int. Ed. 48 (2009) 5897–5899.
[11] Y. Xia, Y. Xiong, B. Lim, S.E. Skrabalak, Shape-controlled synthesis of metal nanocrystals: simple chemistry meets complex physics? Angew. Chem. Int. Ed. 48 (2009) 60–103.
[12] S. Guo, E. Wang, Noble metal nanomaterials: controllable synthesis and application in fuel cells and analytical sensors, Nano Today 6 (2011) 240–264.
[13] M. Yang, A. Javadi, S. Gong, Sensitive electrochemical immunosensor for the detection of cancer biomarker using quantum dot functionalized graphene sheets as labels, Sens. Actuators B 155 (2011) 357–360.
[14] N. Sanaeifar, M. Rabiee, M. Abdolrahim, M. Tahriri, D. Vashaee, L. Tayebi, A novel electrochemical biosensor based on Fe_3O_4 nanoparticles-polyvinyl alcohol composite for sensitive detection of glucose, Anal. Biochem. 519 (2017) 19–26.
[15] X. Chen, J. Zhu, Z. Chen, C. Xu, Y. Wang, C. Yao, A novel bienzyme glucose biosensor based on three-layer Au–Fe_3O_4@SiO_2 magnetic nanocomposite, Sens. Actuators B 159 (2011) 220–228.
[16] S. Zhao, K. Zhang, Y. Bai, W. Yang, C. Sun, Glucose oxidase/colloidal gold nanoparticles immobilized in Nafion film on glassy carbon electrode: direct electron transfer and electrocatalysis, Bioelectrochemistry 69 (2006) 158–163.
[17] D. Zhai, B. Liu, Y. Shi, L. Pan, Y. Wang, W. Li, R. Zhang, G. Yu, Highly sensitive glucose sensor based on Pt nanoparticle/polyaniline hydrogel heterostructures, ACS Nano 7 (2013) 3540–3546.
[18] J. Wang, Carbon-nanotube based electrochemical biosensors: a review, Electroanalysis 17 (2005) 7–14.
[19] A. Guiseppi-Elie, C. Lei, R.H. Baughman, Direct electron transfer of glucose oxidase on carbon nanotubes, Nanotechnology 13 (2002) 559.
[20] T.K. Mudalige, H. Qu, S.W. Linder, Asymmetric flow-field flow fractionation hyphenated ICP-MS as an alternative to cloud point extraction for quantification of silver nanoparticles and silver speciation: application for nanoparticles with a protein corona, Anal. Chem. 87 (2015) 7395–7401.
[21] I. Sondi, B. Salopek-Sondi, Silver nanoparticles as antimicrobial agent: a case study on E-coli as a model for gram-negative bacteria, J. Colloid Interface Sci. 275 (2004) 177–182.
[22] Y.-H. Yu, C.-C.M. Ma, C.-C. Teng, Y.-L. Huang, S.-H. Lee, I. Wang, M.-H. Wei, Electrical, morphological, and electromagnetic interference shielding properties of silver nanowires and nanoparticles conductive composites, Mater. Chem. Phys. 136 (2012) 334–340.
[23] X. Chen, H.J. Schluesener, Silver nanoparticle: a nanoproduct in medical application, Toxicol. Lett. 176 (2008) 1–12.
[24] Y. Jiang, B. Zheng, J. Du, G. Liu, Y. Guo, D. Xiao, Electrophoresis deposition of Ag nanoparticles on TiO_2 nanotube arrays electrode for hydrogen peroxide sensing, Talanta 112 (2013) 129–135.
[25] J.Y. Kim, J.S. Lee, Multiplexed DNA detection with DNA-functionalized silver and silver/gold nanoparticle superstructure probes, Bull. Korean Chem. Soc. 33 (2012) 221–226.
[26] P. Wu, Y. Gao, H. Zhang, C. Cai, Aptamer-guided silver–gold bimetallic nanostructures with highly active surface-enhanced raman scattering for specific detection and near-infrared photothermal therapy of human breast cancer cells, Anal. Chem. 84 (2012) 7692–7699.
[27] N.P. Sardesai, K. Kadimisetty, R. Faria, J.F. Rusling, A microfluidic electrochemiluminescent device for detecting cancer biomarker proteins, Anal. Bioanal. Chem. 405 (2013) 3831–3838.
[28] F. Patolsky, Y. Weizmann, I. Willner, Long-range electrical contacting of redox enzymes by SWCNT connectors, Angew. Chem. Int. Ed. 43 (2004) 2113–2117.
[29] F. Lucarelli, S. Tombelli, M. Minunni, G. Marrazza, M. Mascini, Electrochemical and piezoelectric DNA biosensors for hybridisation detection, Anal. Chim. Acta 609 (2008) 139–159.
[30] I.M. Rust, J.M. Goran, K.J. Stevenson, Amperometric detection of aqueous silver ions by inhibition of glucose oxidase immobilized on nitrogen-doped carbon nanotube electrodes, Anal. Chem. 87 (2015) 7250–7257.
[31] M. Baghayeri, H. Veisi, Fabrication of a facile electrochemical biosensor for hydrogen peroxide using efficient catalysis of hemoglobin on the porous Pd@Fe_3O_4-MWCNT nanocomposite, Biosens. Bioelectron. 74 (2015) 190–198.
[32] X. Li, X. Liu, W. Wang, L. Li, X. Lu, High loading Pt nanoparticles on functionalization of carbon nanotubes for fabricating nonenzyme hydrogen peroxide sensor, Biosens. Bioelectron. 59 (2014) 221–226.
[33] T.T. Baby, S. Ramaprabhu, SiO_2 coated Fe_3O_4 magnetic nanoparticle dispersed multiwalled carbon nanotubes based amperometric glucose biosensor, Talanta 80 (2010) 2016–2022.
[34] C. Gao, X.Y. Yu, S.Q. Xiong, J.H. Liu, X.J. Huang, Electrochemical detection of arsenic(III) completely free from Noble metal: fe_3O_4 microspheres-room temperature ionic liquid composite showing better performance than gold, Anal. Chem. 85 (2013) 2673–2680.
[35] H.P. Peng, R.P. Liang, J.D. Qiu, Facile synthesis of Fe_3O_4@Al_2O_3 core–shell nanoparticles and their application to the highly specific capture of heme proteins for direct electrochemistry, Biosens. Bioelectron. 26 (2011) 3005–3011.
[36] M. Baghayeri, A. Amiri, S. Farhadi, Development of non-enzymatic glucose sensor based on efficient loading Ag nanoparticles on functionalized carbon nanotubes, Sens. Actuators B 225 (2016) 354–362.

[37] M. Fayazi, M.A. Taher, D. Afzali, A. Mostafavi, Preparation of molecularly imprinted polymer coated magnetic multi-walled carbon nanotubes for selective removal of dibenzothiophene, Mater. Sci. Semicond. Process. 40 (2015) 501–507.
[38] M. Baghayeri, M. Namadchian, H. Karimi-Maleh, H. Beitollahi, Determination of nifedipine using nanostructured electrochemical sensor based on simple synthesis of Ag nanoparticles at the surface of glassy carbon electrode: application to the analysis of some real samples, J. Electroanal. Chem. 697 (2013) 53–59.
[39] M. Baghayeri, Glucose sensing by a glassy carbon electrode modified with glucose oxidase and a magnetic polymeric nanocomposite, RSC Adv. 5 (2015) 18267–18274.
[40] S. Wu, H.X. Ju, Y. Liu, Conductive mesocellular silica–carbon nanocomposite foams for immobilization, direct electrochemistry, and biosensing of proteins, Adv. Funct. Mater. 17 (2007) 585–592.
[41] Y.F. Bai, T.B. Xu, J.H. Luong, H.F. Cui, Direct electron transfer of glucose oxidase-boron doped diamond interface: a new solution for a classical problem, Anal. Chem. 86 (2014) 4910–4918.
[42] T. Terse-Thakoor, K. Komori, P. Ramnani, I. Lee, A. Mulchandani, Electrochemically functionalized seamless three dimensional graphene-carbon nanotube hybrid for direct electron transfer of glucose oxidase and bioelectrocatalysis, Langmuir 31 (2015) 13054–13061.
[43] X. Kang, J. Wang, H. Wu, I.A. Aksay, J. Liu, Y. Lin, Glucose oxidase?graphene?chitosan modified electrode for direct electrochemistry and glucose sensing, Biosens. Bioelectron. 25 (2009) 901–905.
[44] R. Devasenathipathy, V. Mani, S.M. Chen, S.T. Huang, T.T. Huang, C.M. Lin, K.Y. Hwa, T.Y. Chen, B.J. Chen, Glucose biosensor based on glucose oxidase immobilized at gold nanoparticles decorated graphene-carbon nanotubes, Enzyme Microb. Technol. 78 (2015) 40–45.
[45] A.P. Periasamy, Y.J. Chang, S.M. Chen, Amperometric glucose sensor based on glucose oxidase immobilized on gelatin-multiwalled carbon nanotube modified glassy carbon electrode, Bioelectrochemistry 80 (2011) 114–120.
[46] V. Mani, R. Devasenathipathy, S.M. Chen, S.T. Huang, V.S. Vasantha, Immobilization of glucose oxidase on graphene and cobalt phthalocyanine composite and its application for the determination of glucose, Enzyme Microb. Technol. 66 (2014) 60–66.
[47] M.A. Kamyabi, N. Hajari, A.P. Turner, A. Tiwari, A high-performance glucose biosensor using covalently immobilized glucose oxidase on a poly(2,6-diaminopyridine)/carbon nanotube electrode, Talanta 116 (2013) 801–808.
[48] A.E. Vilian, V. Mani, S.M. Chen, B. Dinesh, S.T. Huang, The immobilization of glucose oxidase at manganese dioxide particles-decorated reduced graphene oxide sheets for the fabrication of a glucose biosensor, J. Ind. Eng. Chem. 53 (2014) 15582–15589.
[49] S. Palanisamy, C. Karuppiah, S.M. Chen, Direct electrochemistry and electrocatalysis of glucose oxidase immobilized on reduced graphene oxide and silver nanoparticles nanocomposite modified electrode, Colloids Surf. B 114 (2014) 164–169.
[50] F.Y. Kong, S.X. Gu, W.W. Li, T.T. Chen, Q. Xu, W. Wang, A paper disk equipped with graphene/polyaniline/Au nanoparticles/glucose oxidase biocomposite modified screen-printed electrode: toward whole blood glucose determination, Biosens. Bioelectron. 56 (2014) 77–82.
[51] T. Homma, D. Sumita, M. Kondo, T. Kuwahara, M. Shimomura, Amperometric glucose sensing with polyaniline/poly(acrylic acid) composite film bearing covalently-immobilized glucose oxidase: a novel method combining enzymatic glucose oxidation and cathodic O_2 reduction, J. Electroanal. Chem. 712 (2014) 119–123.
[52] H. Razmi, R. Mohammad-Rezaei, Graphene quantum dots as a new substrate for immobilization and direct electrochemistry of glucose oxidase: application to sensitive glucose determination, Biosens. Bioelectron. 41 (2013) 498–504.
[53] Q. Xu, S.X. Gu, L. Jin, Y.E. Zhou, Z. Yang, W. Wang, X. Hu, Graphene/polyaniline/gold nanoparticles nanocomposite for the direct electron transfer of glucose oxidase and glucose biosensing, Sens. Actuators B 190 (2014) 562–569.
[54] Z. Nasri, E. Shams, A glucose biosensor based on direct electron transfer of glucose oxidase immobilized onto glassy carbon electrode modified with nitrophenyl diazonium salt, Electrochim. Acta 112 (2013) 640–647.
[55] X. Kang, Z. Mai, X. Zou, P. Cai, J. Mo, A novel glucose biosensor based on immobilization of glucose oxidase in chitosan on a glassy carbon electrode modified with gold-platinum alloy nanoparticles/multiwall carbon nanotubes, Anal. Biochem. 369 (2007) 71–79.
[56] Y. Liu, D. Yu, C. Zeng, Z. Miao, L. Dai, Biocompatible graphene oxide-based glucose biosensors, Langmuir 26 (2010) 6158–6160.

Biographies

Mehdi Baghayeri is an Associate Professor in the Department of Science, Hakim Sabzevari University, Sabzevar, Iran. He received his Ph.D. from University of Mazandaran, Babolsar, Iran in 2012. His main research interests are focused on bioelectrochemistry and nanobiotechnology.

Hojat Veisi is an Associate Professor in the Department of Chemistry, Payame Noor University, Tehran, Iran. He received his Ph.D. from University of Bu-Ali Sina University, Hamedan, Iran in 2009. His main research interests are focused on synthesis of nanocatalysts and nanobiotechnology.

Masoud Ghanei-Motlagh is a Ph.D. Candidate in Analytical Chemistry, Shahid Bahonar University of Kerman, Iran. His research interests include synthesis and applications of the novel nanomaterials and also development of electrochemical sensor for environmental applications.